

Supplementary Material

Influence of the cobalt content in cobalt iron oxides on the electrocatalytic OER activity

*Sascha Saddeler, Georg Bendt, Soma Salamon, Felix T. Haase, Joachim Landers, Janis Timoshenko, Clara Rettenmaier, Hyo Sang Jeon, Arno Bergmann, Heiko Wende, Beatriz Roldan Cuenya and Stephan Schulz**

Content

I. Material Characterization

Table S1. EDX data and calculated amounts for $x = 0-3$.

Figure S1. Rietveld refinement for $x = 1.75-2.75$.

Table S2. Amounts of spinel and rock-salt structure and their lattice parameters for $x = 1.75-2.75$ extracted from Rietveld-refinement.

Figure S2. Histograms for $x = 0, 0.50, 1.00, 1.50, 2.00$ and 2.50 .

Table S3. Particle sizes calculated with use of the Scherrer equation and from TEM measurements.

Figure S3. XPS spectra of the Co 2p and Fe 2p regions of $\text{Co}_x\text{Fe}_{3-x}\text{O}_4$ nanoparticles for $x = 0.50$ (a), 1.00 (b), 1.50 (c) and 1.75 (d), 2.25 (e) and 2.50 (f).

Figure S4. a) Raman spectra ($P = 1.50$ mW) of as-prepared cobalt ferrite $\text{Co}_x\text{Fe}_{3-x}\text{O}_4$ ($x \leq 1.75$) and cobalt-rich wustite nanoparticles ($\text{Co}_{x/3}\text{Fe}_{(1-x)/3}\text{O}$ ($x \geq 2$)) and b) influence of the laser power (0.15 and 1.50 mW) on the obtained spectra for biphasic mixtures $x = 2-3$.

Figure S5. FT-IR spectra of as-prepared cobalt ferrite $\text{Co}_x\text{Fe}_{3-x}\text{O}_4$ ($x \leq 1.75$) and cobalt-rich wustite nanoparticles ($\text{Co}_{x/3}\text{Fe}_{(1-x)/3}\text{O}$ ($x \geq 2$)) and surfactants.

Figure S6. (a) Magnetization curves $M(H)$ recorded for $\text{Co}_x\text{Fe}_{3-x}\text{O}_4$ ($x = 1.25-2.5$) nanoparticles at 4.3 K (a) and 300 K (b).

Figure S7. Temperature-dependent magnetization curves $M(T)$ recorded for $\text{Co}_x\text{Fe}_{3-x}\text{O}_4$ ($x = 1.25-2.5$) nanoparticles at 10 mT between 4.3 K and 320 K with a sweep rate of 2 K min^{-1} following the ZFC-FC protocol, (a) full view (b) closeup of $x = 2.25-2.5$.

Figure S8. Linear sweep voltammograms for CoFe_2O_4 ($x = 1$) with a Pt and a graphite counter electrode.

Figure S9. Linear sweep voltammograms for CoFe_2O_4 ($x = 1$) with catalyst loadings of $50, 100$ and 200 $\mu\text{g}/\text{cm}^2$ before and after 100 cycles.

Figure S10. Tafel plots for $x = 0-1.00$ (a) and $1.25-3.00$ (b).

Figure S11. Chronoamperometry measurement of CoFe_2O_4 ($x = 1$) at 1 mA/cm^2 over 48 h.

Figure S12. (a) X-ray absorption edge positions at the Co-K edge for cobalt oxide reference compounds ($rs\text{-Co}^{+2}\text{O}$, $w\text{-Co}^{+2}\text{O}$, $\beta\text{-Co}^{+2}(\text{OH})_2$, $\text{Co}^{+2.67}_3\text{O}_4$ and CoOOH) with linear calibration 2.6 ± 0.1 eV/ox. state + 7713.1 ± 0.3 eV. (b) X-ray absorption edge positions at the Fe-K edge for iron oxide reference compounds (FeO , $\text{Fe}^{+2.67}_3\text{O}_4$, Fe^{+3}OOH , $\text{Fe}^{+3}_2\text{O}_3$) with linear calibration 3.3 ± 0.2 eV/Ox.State + 7113.8 ± 0.5 eV.

Figure S13. (a) XANES Co K-edge spectra of $\text{CoO}_x(\text{OH})_y$ references for oxidation state calibration and comparison. (b) XANES Fe K-edge spectra of reference compounds used for calibration and comparison.

Figure S14. Operando XANES at Co K- and Fe K-edge of CoFe_2O_4 (a, d), $\text{Co}_{0.25}\text{Fe}_{2.75}\text{O}_4$ (b, e) and CoO_x (c) NPs. The spectra were recorded dry, as-prepared, during OER at $1.8 V_{\text{RHE}}$ and after OER at $1 V_{\text{RHE}}$ in 0.1M KOH . Panel (f) shows the Fe oxidation state for $\text{Co}_{2.25}\text{Fe}_{0.75}\text{O}_4$, CoFe_2O_4 and $\text{Co}_{0.25}\text{Fe}_{2.75}\text{O}_4$.

Figure S15. Co and Fe K-edge EXAFS in R- and k-space of Co_3O_4 and Fe_3O_4 references.

Figure S16. *Operando* EXAFS with fits at the Co (top row) and Fe (bottom row) K-edge of $\text{Co}_{2.25}\text{Fe}_{0.75}\text{O}_4$ (a, e), CoFe_2O_4 (b, f), $\text{Co}_{0.25}\text{Fe}_{2.75}\text{O}_4$ (c, g) and CoO_x (d) NPs. The spectra were recorded as-prepared, during OER at $1.8 V_{\text{RHE}}$ and after OER at $1 V_{\text{RHE}}$ in 0.1M KOH.

Figure S17. Co K-edge EXAFS spectra of CoO_x NPs in k-space measured as-prepared (ap), during OER at $+1.8 V_{\text{RHE}}$ and after OER at $+1 V_{\text{RHE}}$ in 0.1M KOH.

Figure S18. Co and Fe K-edge EXAFS in k-space of $\text{Co}_x\text{Fe}_y\text{O}_4$ NPs with varying composition measured as-prepared, during OER at $+1.8 V_{\text{RHE}}$ and after OER at $+1 V_{\text{RHE}}$ in 0.1M KOH.

Table S4: Oxidation state and absorption edge position in eV for CoO_x reference compounds and $\text{Co}_x\text{Fe}_y\text{O}_4$ NPs with different composition as-prepared, after activation cycling, during OER and after OER.

Table S5: Oxidation state and absorption edge position in eV for FeO_x reference compounds and $\text{Co}_x\text{Fe}_y\text{O}_4$ NPs with varying composition as-prepared, after activation cycling, during OER and after OER.

Table S6: Co_3O_4 and Fe_3O_4 reference compounds.

II. Experimental

Table S7. Amounts of used $\text{Co}(\text{acac})_2$ and $\text{Fe}(\text{acac})_3$ for the synthesis of $\text{Co}_x\text{Fe}_{3-x}\text{O}_4$ nanoparticles.

III. References

I. Material Characterization

Table S1. EDX data and calculated ratios for $x = 0-3$.

x	measured		calculated	
	Co / at%	Fe / at %	Co / at%	Fe / at %
0	0	100	0	100
0.25	6.89 ± 0.29	93.11 ± 2.05	8.33	91.67
0.50	14.73 ± 0.60	85.27 ± 2.20	16.67	83.33
0.75	23.61 ± 0.97	76.39 ± 2.19	25.00	75.00
1.00	32.03 ± 1.11	66.79 ± 1.67	33.33	66.67
1.25	43.21 ± 0.66	56.79 ± 0.80	41.67	58.33
1.50	52.57 ± 0.30	47.43 ± 0.35	50.00	50.00
1.75	55.25 ± 1.04	44.75 ± 1.34	58.33	41.67
2.00	65.46 ± 0.85	34.54 ± 1.60	66.67	33.33
2.25	74.27 ± 0.67	25.73 ± 1.76	75.00	25.00
2.50	83.54 ± 0.48	16.46 ± 1.96	83.33	16.67
2.75	92.31 ± 0.29	7.69 ± 2.26	91.67	8.33
3.00	100	0	100	0

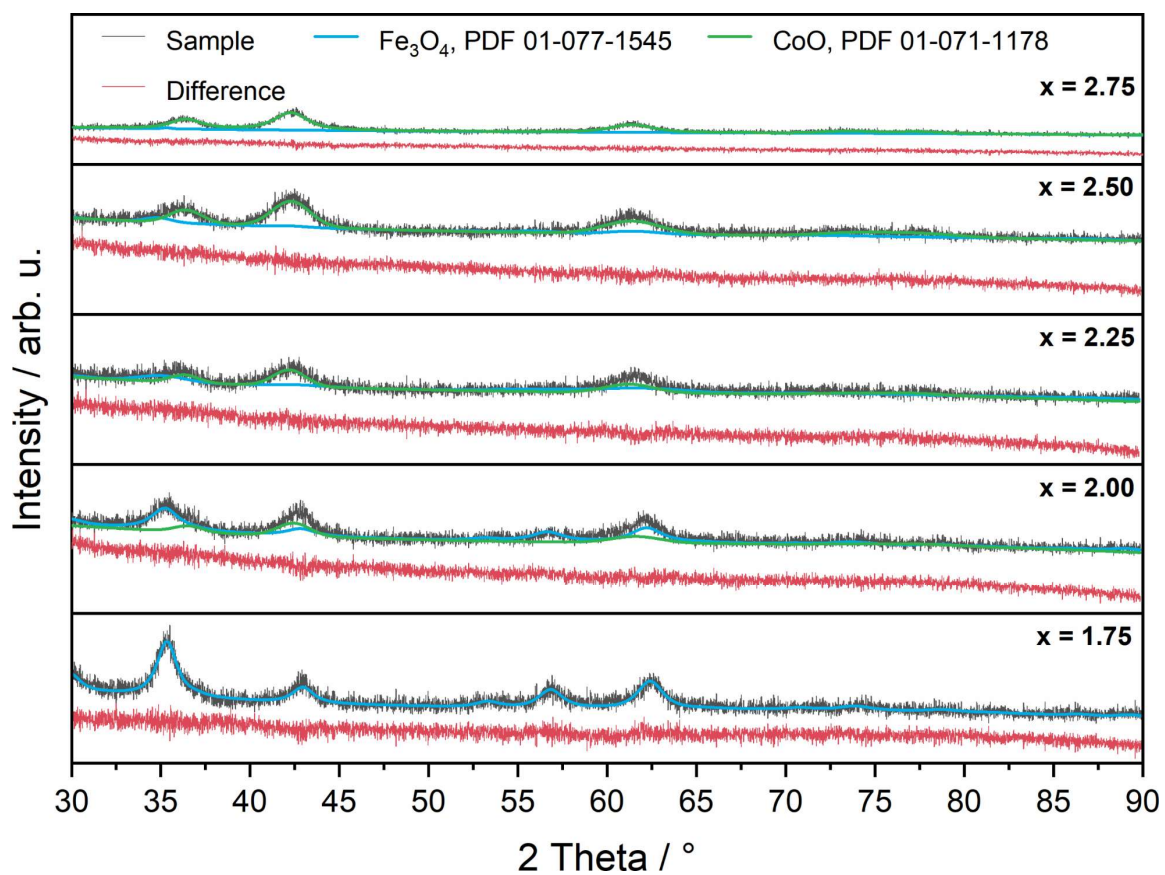


Figure S1. Rietveld refinement for $x = 1.75\text{--}2.75$.

Table S2. Amounts of spinel and rock-salt structure and their lattice parameters for $x = 1.75\text{--}2.75$ extracted from Rietveld-refinement.

x	Amount / %		Lattice parameters / Å	
	Spinel structure	Rock-salt structure	Spinel structure	Rock-salt structure
1.75	100	0	8.414	/
2.00	70	30	8.437	4.250
2.25	42	57	8.460	4.258
2.50	10	90	8.550	4.270
2.75	1	99	8.420	4.280

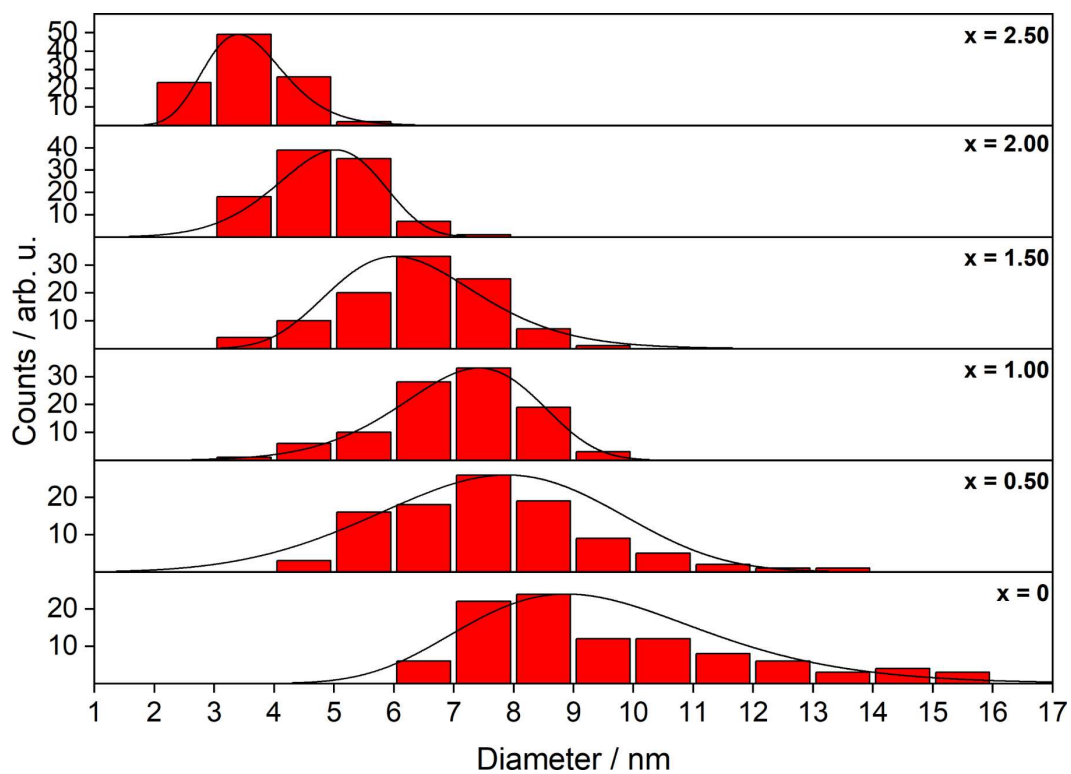


Figure S2. Histograms for $x = 0, 0.50, 1.00, 1.50, 2.00$ and 2.50 .

Table S3. Particle sizes calculated with use of the Scherrer equation and from TEM measurements.

x	d (XRD) / nm	d (TEM) / nm
0	7.5	8.9 ± 2.3
0.50	8.1	7.6 ± 1.8
1.00	6.6	7.2 ± 1.2
1.50	4.6	6.4 ± 1.2
2.00	4.4	4.8 ± 0.8
2.50	3.5	3.4 ± 0.7

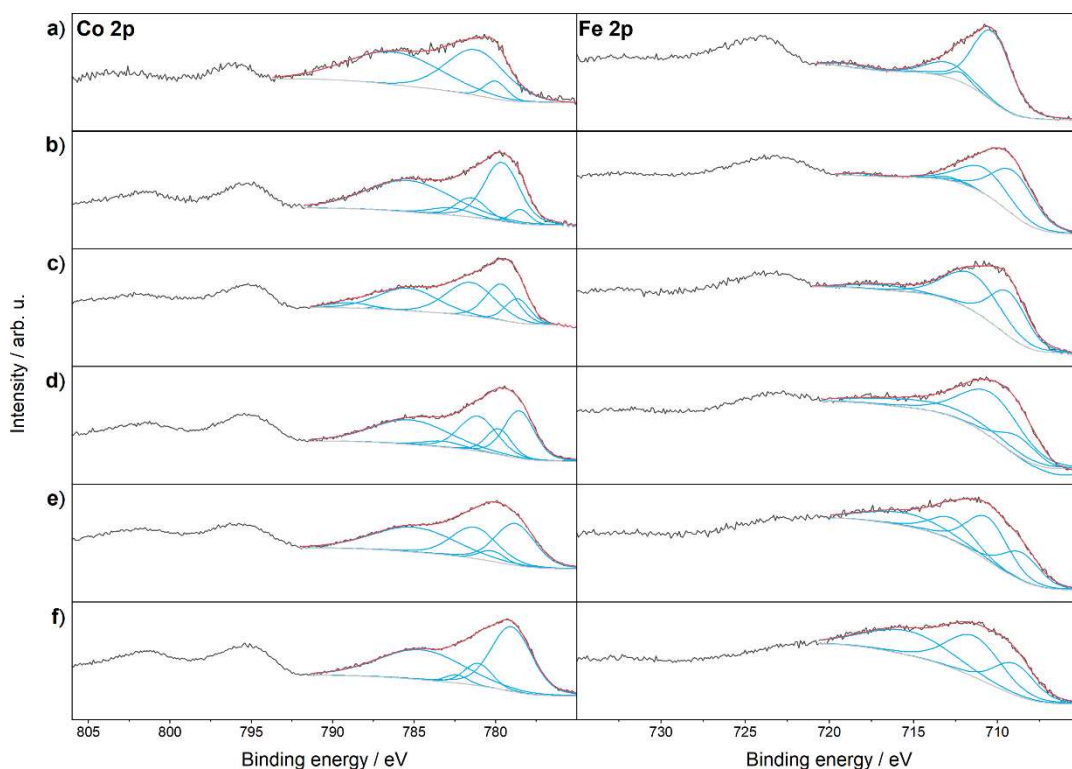


Figure S3. XPS spectra of the Co 2p and Fe 2p regions of $\text{Co}_x\text{Fe}_{3-x}\text{O}_4$ nanoparticles for $x = 0.50$ (a), 1.00 (b), 1.50 (c) and 1.75 (d), 2.25 (e) and 2.50 (f).

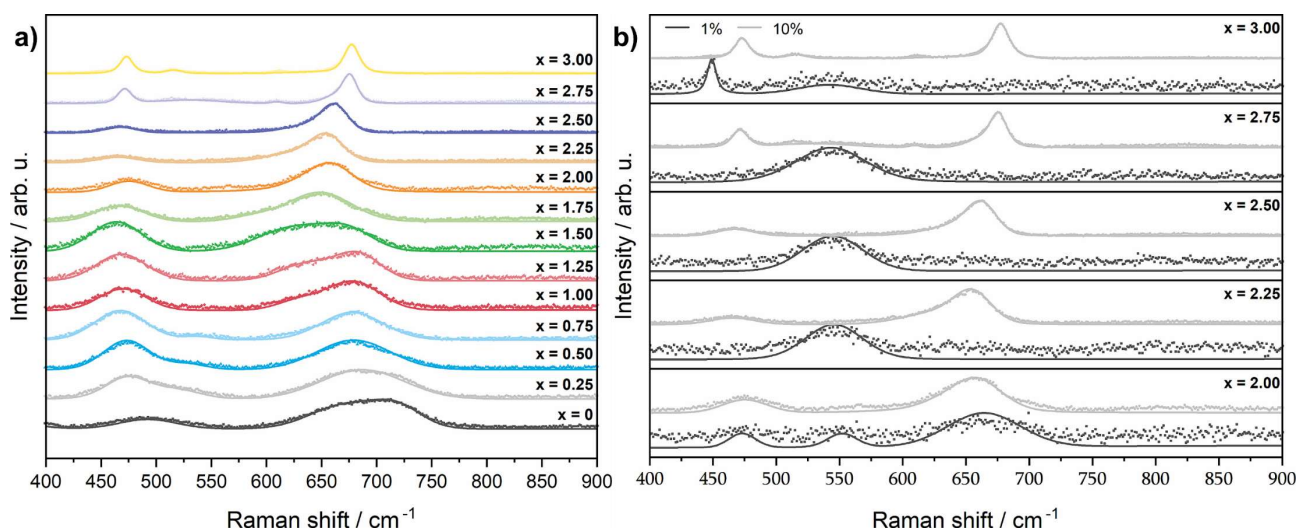


Figure S4. a) Raman spectra ($P = 1.50$ mW) of as-prepared cobalt ferrite $\text{Co}_x\text{Fe}_{3-x}\text{O}_4$ ($x \leq 1.75$) and cobalt-rich wustite nanoparticles ($\text{Co}_{x/3}\text{Fe}_{(1-x)/3}\text{O}$ ($x \geq 2$)) and b) influence of the laser power (0.15 and 1.50 mW) on the obtained spectra for biphasic mixtures $x = 2-3$.

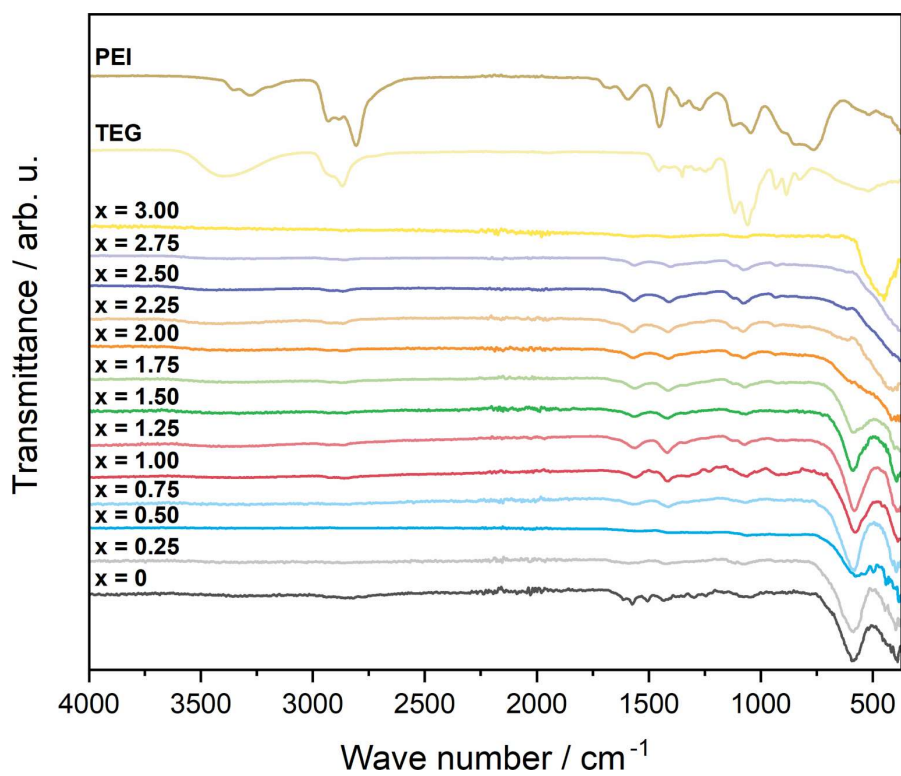


Figure S5. FT-IR spectra of as-prepared cobalt ferrite $\text{Co}_x\text{Fe}_{3-x}\text{O}_4$ ($x \leq 1.75$) and cobalt-rich wustite nanoparticles ($\text{Co}_{x/3}\text{Fe}_{(1-x)/3}\text{O}$ ($x \geq 2$)) and surfactants.

Magnetometry

Field-dependent magnetization curves recorded for $\text{Co}_x\text{Fe}_{3-x}\text{O}_4$ ($x = 1.25\text{--}2.5$) nanoparticles at 4.3 K (Fig. S6a) display a wide hysteresis with coercive fields $H_c \geq 1$ T, as expected for CoFe_2O_4 -related systems. High magnetization values $M_{(4.3\text{K},9\text{T})}$ of ca. $77 \text{ Am}^2 \text{ kg}^{-1}$ for $x = 1.25$ substantiate the finding from in-field Mössbauer spectroscopy regarding a rather random ion site occupation, showing only a minor Co B-site preference. Due to the lower magnetic moment of Co^{3+} as compared to Fe^{3+} and considering the finding of spin canting angles in the range of $20\text{--}25^\circ$ at 5 T, an even higher saturation magnetization is expected for CoFe_2O_4 ,^[1,2] which can be explained by a reduced canceling of A- and B-site sublattice magnetization due to the transfer of Fe^{3+} to the dominant B-site lattice in comparison to a perfectly ordered inverse spinel.^[3,4]

A minor contribution with very low coercive fields was found, likely to originate from the smallest particles in the studied sample material, where the strongly limited magnetic volume leads to diminished remanence, despite the materials' high magnetocrystalline anisotropy. In general, upon moving to higher Co-content, a stark decrease in magnetization is visible, in agreement with the exceedingly antiferromagnetic ordering pertaining to these samples. The lack of magnetic orientation at $x \geq 2$ agrees with the spin-canting observed in Mössbauer spectra, indicating a random orientation of spins. At room temperature (Fig. S6b), no hysteresis is observable, presumably due to superparamagnetic relaxation of the nanoparticles net magnetic moment at elevated temperatures.

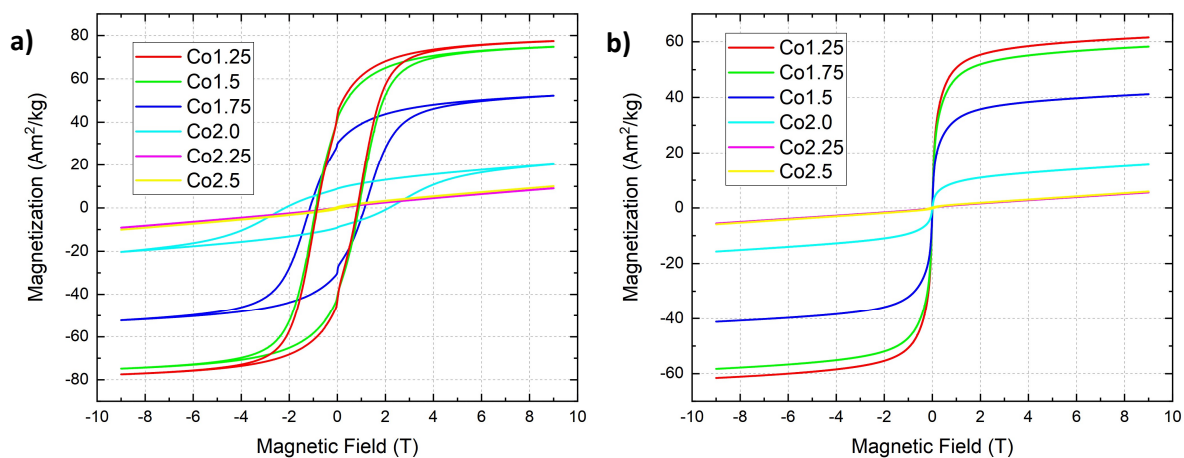


Figure S6. (a) Magnetization curves $M(H)$ recorded for $\text{Co}_x\text{Fe}_{3-x}\text{O}_4$ ($x = 1.25\text{--}2.5$) nanoparticles at 4.3 K (a) and 300K (b).

Temperature-dependent ZFC-FC magnetization curves (Fig. S7) are characteristic for the transition from the magnetically blocked to the superparamagnetic state, with blocking temperatures in the range of ca. 150-200 K for x ca. 1.25–1.75. For higher Co-content, very minor features are observed with decreasing temperature, which could be connected to the Néel transition, being in the range of 30-40 K for pure Co_3O_4 .^[5] No features of the magnetization curves could be assigned clearly to an additional phase transition, which would correspond to the Néel temperature of a wustite (cobalto-wustite) phase.

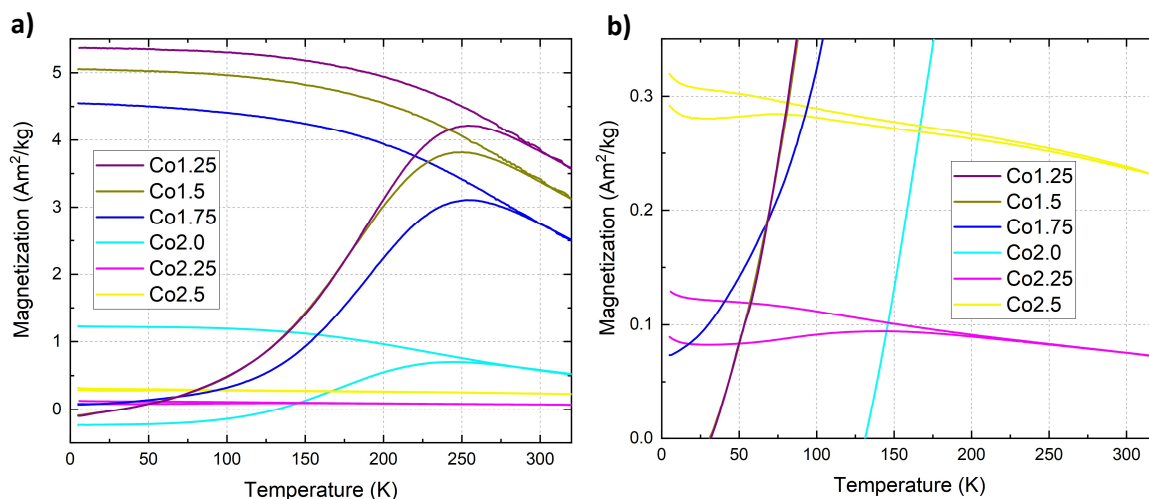


Figure S7. Temperature-dependent magnetization curves $M(T)$ recorded for $\text{Co}_x\text{Fe}_{3-x}\text{O}_4$ ($x = 1.25\text{--}2.5$) nanoparticles at 10 mT between 4.3 K and 320 K with a sweep rate of 2 K min^{-1} following the ZFC-FC protocol, (a) full view (b) closeup of $x = 2.25\text{--}2.5$

OER Activity

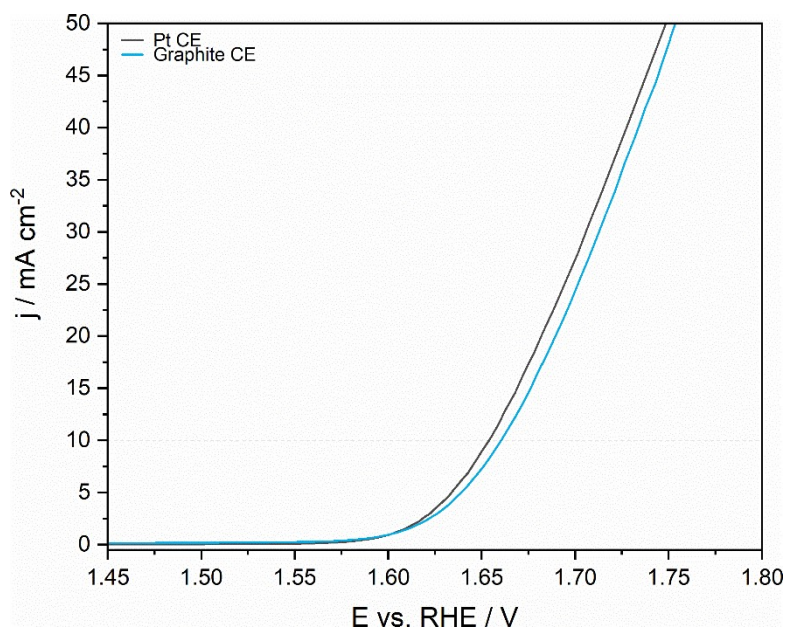


Figure S8. Linear sweep voltammograms for CoFe_2O_4 ($x = 1$) with a Pt and a graphite counter electrode.

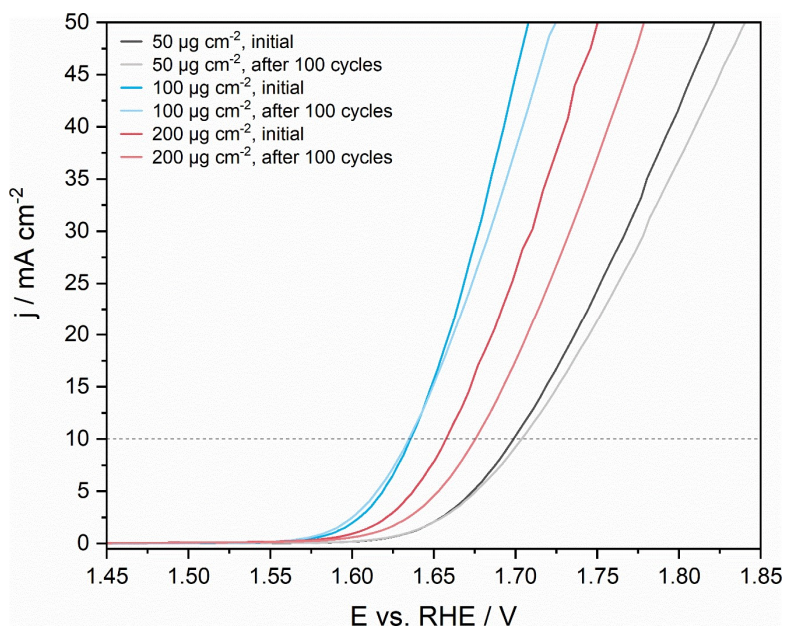


Figure S9. Linear sweep voltammograms for CoFe_2O_4 ($x = 1$) with catalyst loadings of 50, 100 and 200 $\mu\text{g}/\text{cm}^2$ before and after 100 cycles.

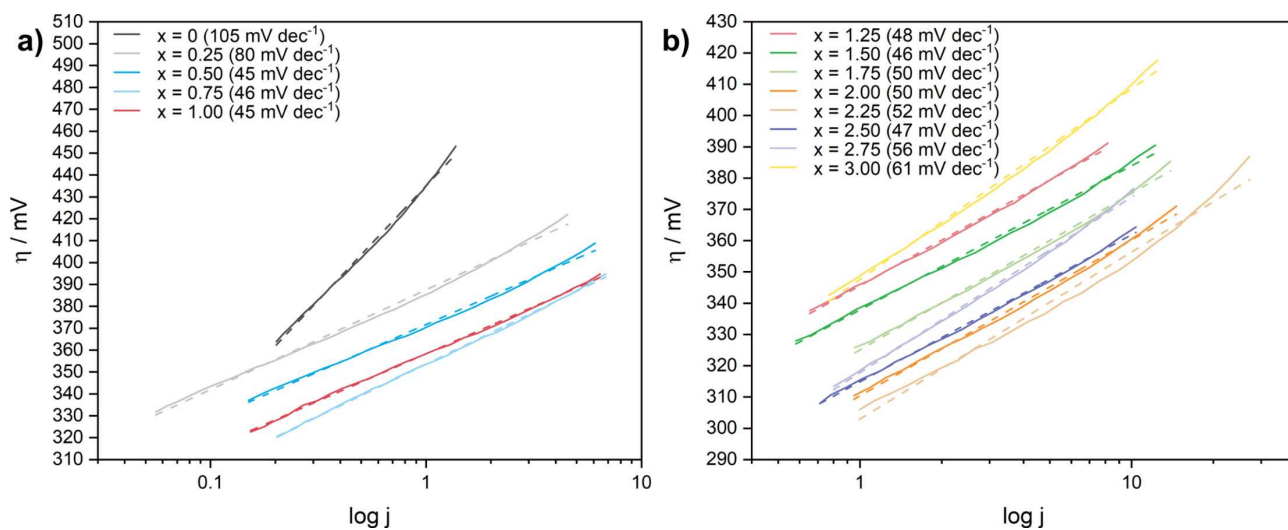


Figure S10. Tafel plots for $x = 0-1.00$ (a) and $1.25-3.00$ (b).

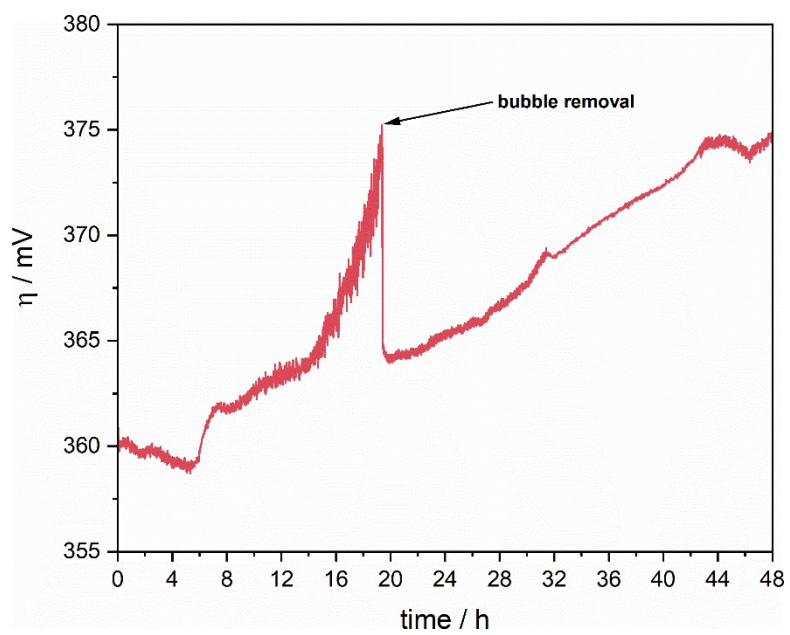


Figure S11. Chronoamperometry measurement of CoFe_2O_4 ($x = 1$) at 1 mA/cm^2 over 48 h.

X-ray absorption spectroscopy

XAS measurements were carried out at PETRA III P64 Advanced EXAFS beamline at DESY. Samples were measured dry and *operando* at the Co (7708.9 eV) and Fe (7112.0 eV) K-edges using a self-made electrochemical cell and 0.1 M KOH as electrolyte. The counter electrode was a Pt mesh and the reference electrode a leak-free Ag/AgCl electrode. All spectra were acquired under stationary conditions. The fluorescence yield signal was detected by a 100-pixel high-purity Ge detector. The catalysts were deposited as an ink on carbon paper (GDE, FuelCellStore). The first measurements were conducted dry, in as-prepared state. After a conditioning with 20 cyclic voltammograms from 1 to 1.8 V_{RHE} and 50 mV/s scan rate, the potential was ramped up to 1.8 V_{RHE}. There, the potential was held, and the catalysts were measured during OER. Finally, the samples were measured after OER at 1.0 V_{RHE}. All potentials were applied along with iR-correction extracted from potentiometric-electrochemical impedance spectroscopy measurements at 1 V_{RHE}.

The XANES edge position was determined by integration of the absorption edge with the resulting edge position in eV. The calibration of the oxidation states using cobalt- and iron-oxide reference compounds with known oxidation state and their respective edge position was used to calculate the average oxidation states for all measurements. The error of the fit and the oxidation state was ± 0.1 for Co and ± 0.2 for Fe.

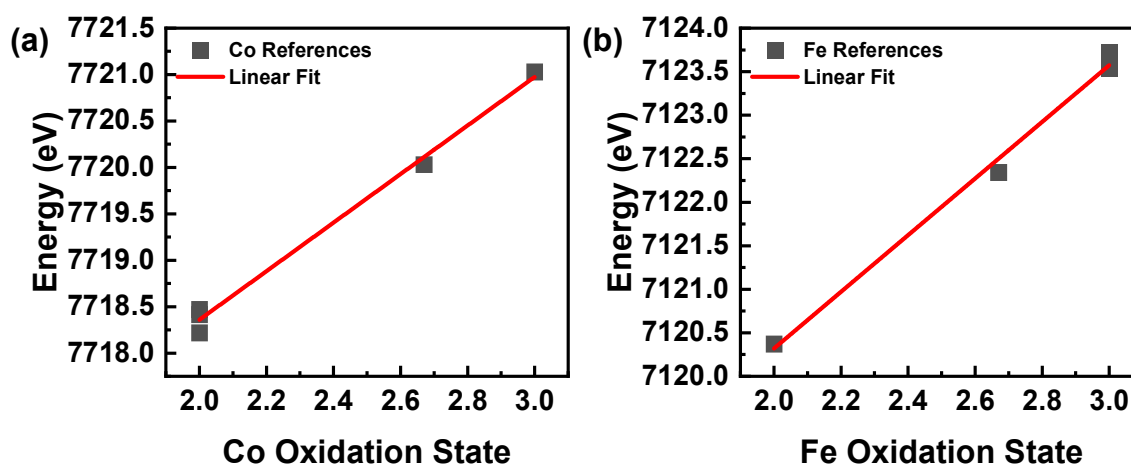


Figure S12. (a) X-ray absorption edge positions at the Co-K edge for cobalt oxide reference compounds (*rs*-Co⁺²O, *w*-Co⁺²O, β -Co⁺²(OH)₂, Co^{+2.67}₃O₄ and CoOOH) with linear calibration 2.6 ± 0.1 eV/ox. state + 7713.1 ± 0.3 eV. (b) X-ray absorption edge positions at the Fe-K edge for iron oxide reference compounds (FeO, Fe^{+2.67}₃O₄, Fe⁺³OOH, Fe⁺³₂O₃) with linear calibration 3.3 ± 0.2 eV/Ox.State + 7113.8 ± 0.5 eV.

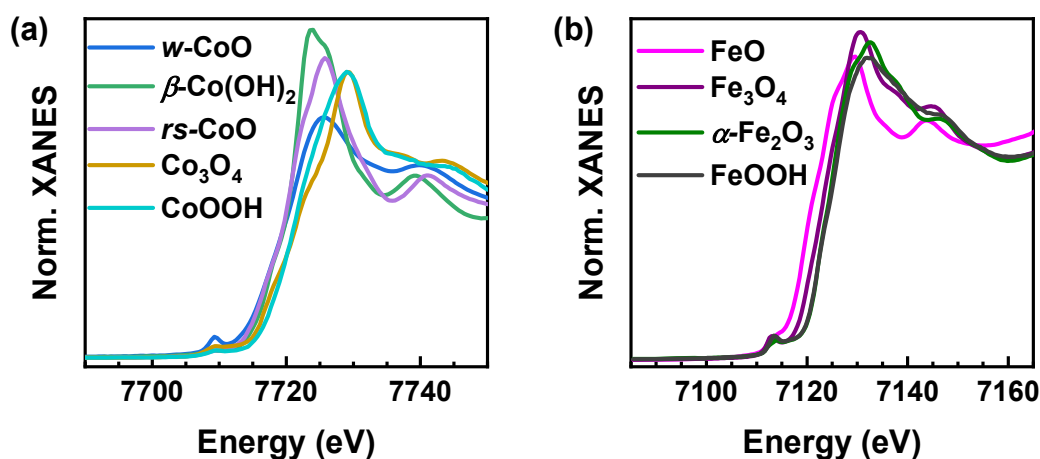


Figure S13. (a) XANES Co K-edge spectra of $\text{CoO}_x(\text{OH})_y$ references for oxidation state calibration and comparison. (b) XANES Fe K-edge spectra of reference compounds used for calibration and comparison.

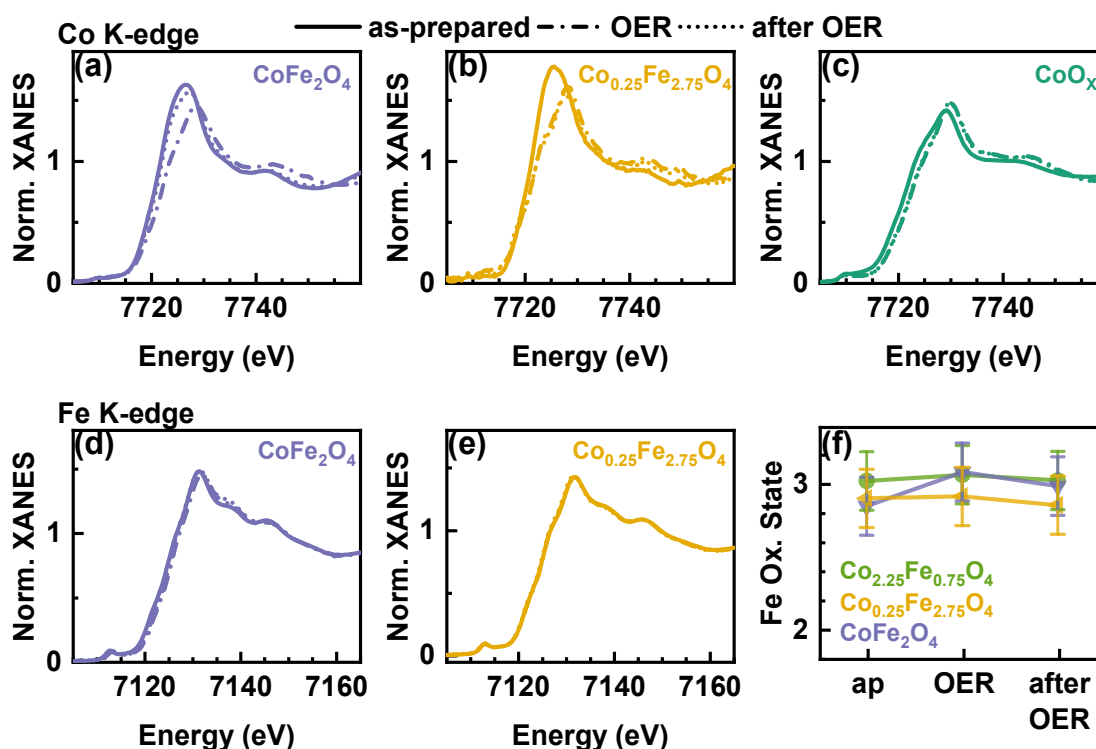


Figure S14. Operando XANES at Co K- and Fe K-edge of CoFe_2O_4 (a, d), $\text{Co}_{0.25}\text{Fe}_{2.75}\text{O}_4$ (b, e) and CoO_x (c) NPs. The spectra were recorded dry, as-prepared, during OER at $1.8 V_{\text{RHE}}$ and after OER at $1 V_{\text{RHE}}$ in 0.1M KOH . Panel (f) shows the Fe oxidation state for $\text{Co}_{2.25}\text{Fe}_{0.75}\text{O}_4$, CoFe_2O_4 and $\text{Co}_{0.25}\text{Fe}_{2.75}\text{O}_4$.

EXAFS Analysis

For the EXAFS analysis, the variable "x" was introduced which is the fraction of Co or Fe in tetrahedral sites from the overall sum of Co or Fe. The first three main paths were fitted, and the amplitudes A were calculated as follows:

$$A_{M-O}: (6-2x)$$

$$A_{M-M1}: (6-6x)$$

$$A_{M-M2}: (6+10x)$$

This model is extended to two variables x_{Co} and x_{Fe} to fit both edges simultaneously to consider the spinel structure. The variable x_{Fe} depends on the concentration "w" of cobalt from the total number of metal atoms.

$$x_{Fe} = (1/3 - x_{Co} * w) / (1 - w)$$

The advantage of this model is that it provides a quantitative estimation of cobalt or iron in octahedral and tetrahedral sites which provides information of the structure and site occupancy. For $Co_{0.25}Fe_{2.75}O_4$ the concentration of cobalt is very low, and the enhanced x model was not used. Instead, the Fe edge was fitted using a x model as for Fe_3O_4 , and the Co edge was fitted without constrains.

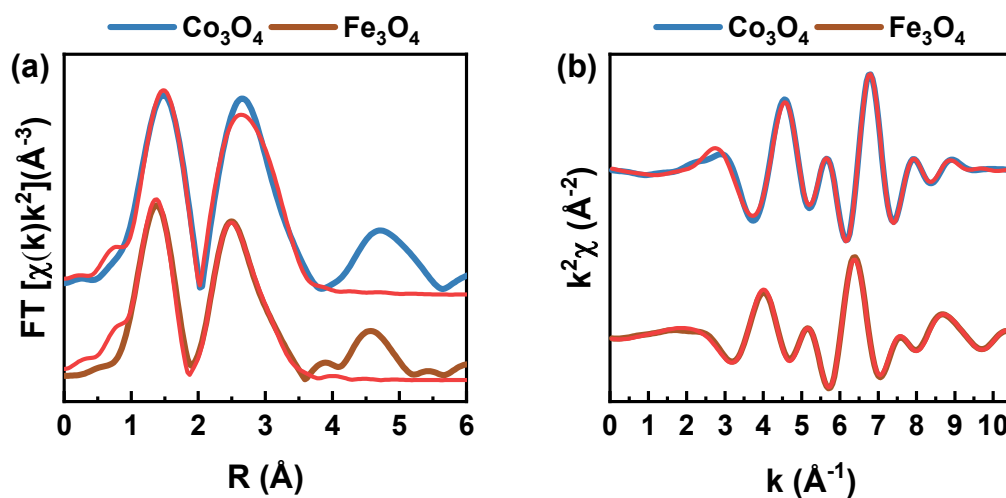


Figure S15. Co and Fe K-edge EXAFS in R- and k-space of Co_3O_4 and Fe_3O_4 references.

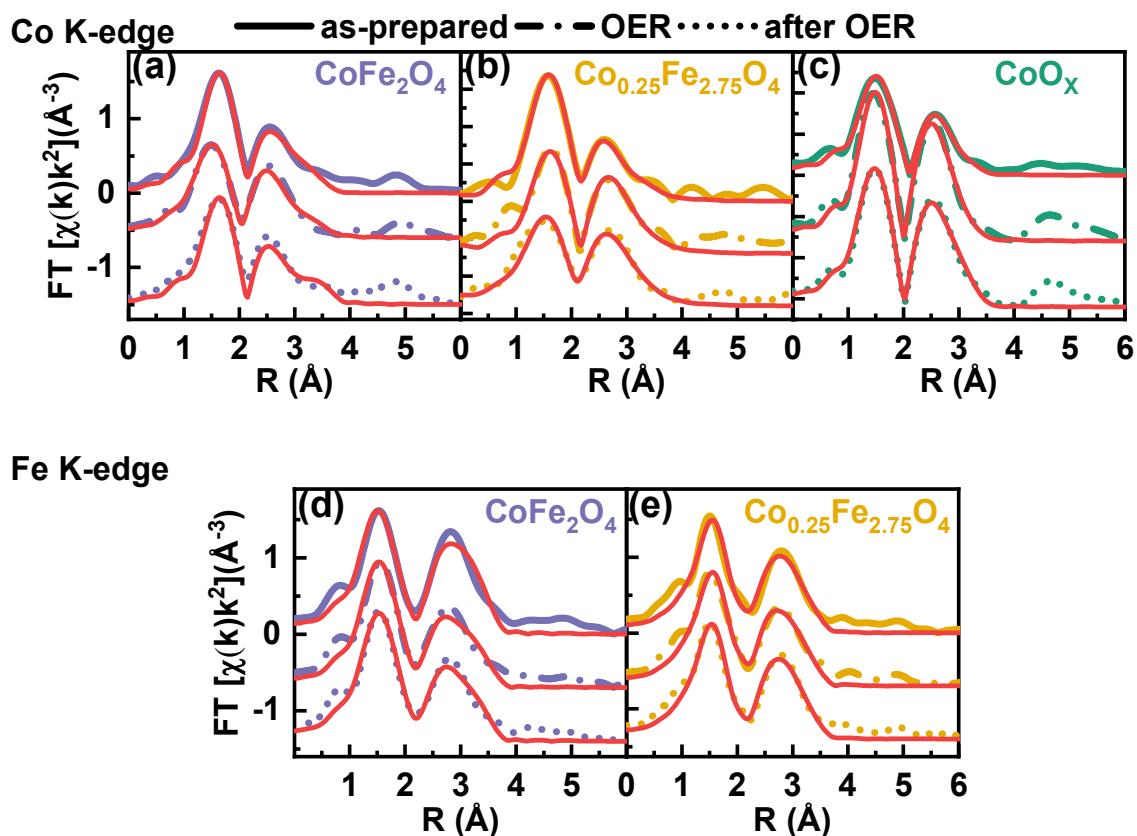


Figure S16. Operando EXAFS with fits at the Co (top row) and Fe (bottom row) K-edge of $\text{Co}_{0.25}\text{Fe}_{0.75}\text{O}_4$ (a, e), CoFe_2O_4 (b, f), $\text{Co}_{0.25}\text{Fe}_{2.75}\text{O}_4$ (c, g) and CoO_x (d) NPs. The spectra were recorded as-prepared, during OER at 1.8 V_{RHE} and after OER at 1 V_{RHE} in 0.1M KOH.

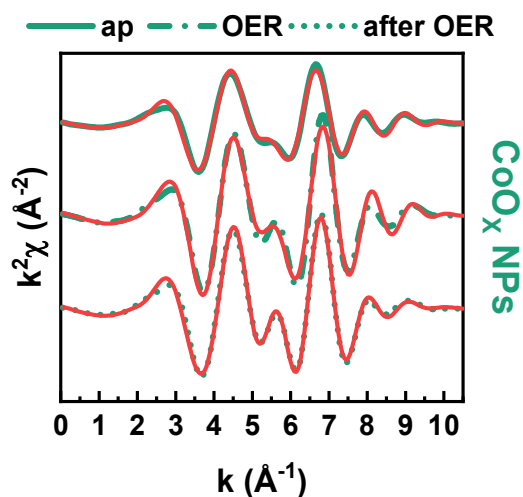


Figure S17. Co K-edge EXAFS spectra of CoO_x NPs in k-space measured as-prepared (ap), during OER at +1.8 V_{RHE} and after OER at +1 V_{RHE} in 0.1M KOH.

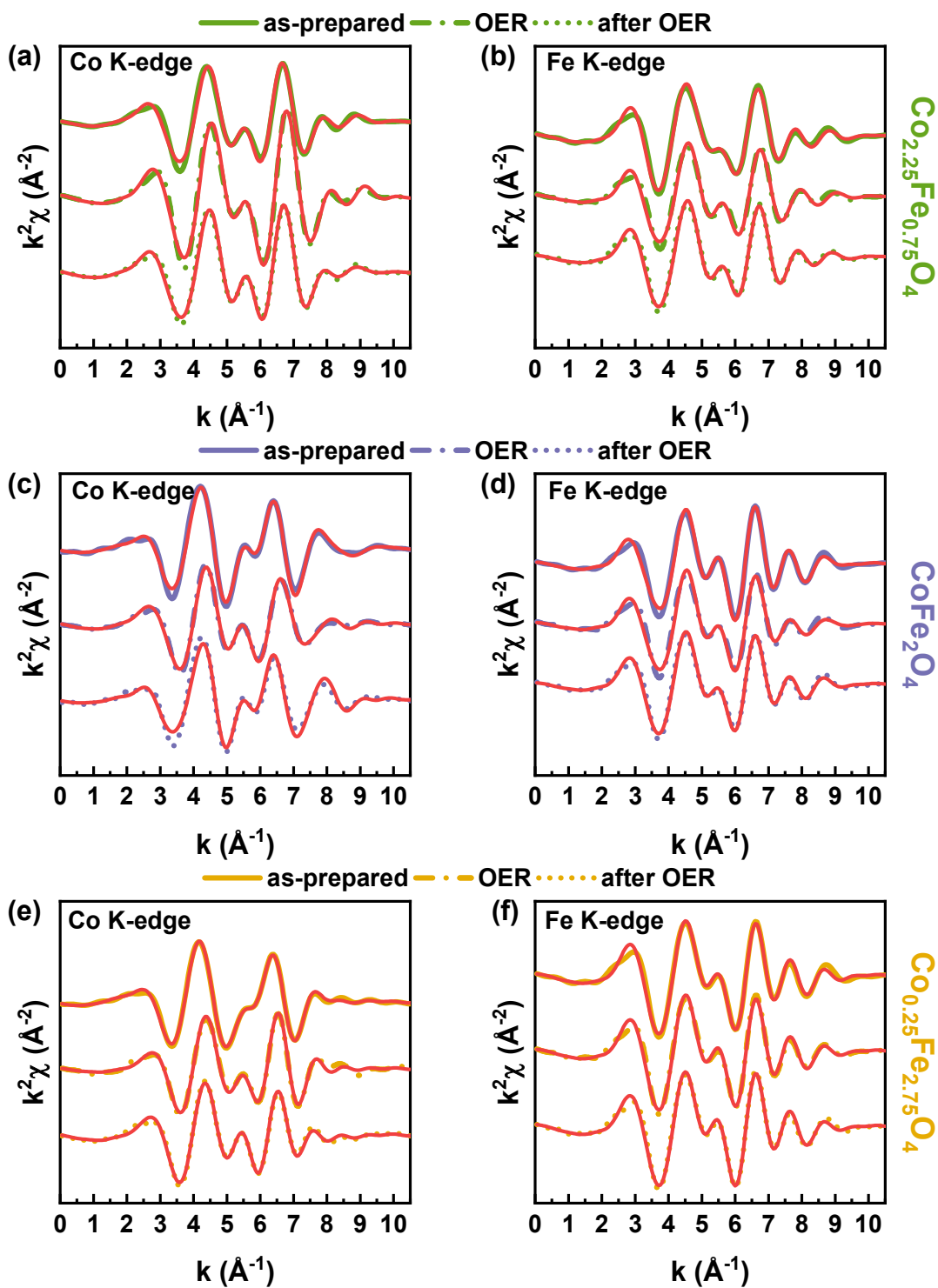


Figure S18. Co and Fe K-edge EXAFS in k-space of $\text{Co}_x\text{Fe}_y\text{O}_4$ NPs with varying composition measured as-prepared, during OER at +1.8 V_{RHE} and after OER at +1 V_{RHE} in 0.1M KOH.

Table S4: Oxidation state and absorption edge position in eV for CoO_x reference compounds and Co_xFe_yO₄ NPs with different composition as-prepared, after activation cycling, during OER and after OER.

Co K-Edge	#	Oxidation State	Edge Position (eV)
References	<i>rs</i> -CoO	2	7718.22
	<i>w</i> -CoO	2	7718.41
	β -Co(OH) ₂	2	7718.47
	Co ₃ O ₄ (Sigma Aldrich)	2.67	7720.03
	CoOOH	3	7721.03
CoO _x	as-prepared	2.5 ± 0.1	7719.78
	at 1.8 V _{RHE} (OER)	3.0 ± 0.1	7720.99
	after OER	3.0 ± 0.1	7720.87
Co _{2.25} Fe _{0.75} O ₄	as-prepared	2.5 ± 0.1	7719.55
	at 1.8 V _{RHE} (OER)	3.0 ± 0.1	7720.99
	after OER	2.7 ± 0.1	7720.14
CoFe ₂ O ₄	as-prepared	2.4 ± 0.1	7719.42
	at 1.8 V _{RHE} (OER)	2.8 ± 0.1	7720.56
	after OER	2.5 ± 0.1	7719.68
Co _{0.25} Fe _{2.75} O ₄	as-prepared	2.3 ± 0.1	7719.08
	at 1.8 V _{RHE} (OER)	2.4 ± 0.1	7719.48
	after OER	2.4 ± 0.1	7719.34

Table S5: Oxidation state and absorption edge position in eV for FeO_x reference compounds and Co_xFe_yO₄ NPs with varying composition as-prepared, after activation cycling, during OER and after OER.

Fe K-Edge	#	Oxidation State	Edge Position (eV)
References	FeO	2	7120.37
	Fe ₃ O ₄	2.67	7122.34
	α-Fe ₂ O ₃	3	7123.54
	FeOOH	3	7123.71
Co _{2.25} Fe _{0.75} O ₄	as-prepared	3.0 ± 0.2	7123.63
	at 1.8 V _{RHE} (OER)	3.0 ± 0.2	7123.77
	after OER	3.0 ± 0.2	7123.65
CoFe ₂ O ₄	as-prepared	2.8 ± 0.2	7123.07
	at 1.8 V _{RHE} (OER)	3.1 ± 0.2	7123.83
	after OER	3.0 ± 0.2	7123.52
Co _{0.25} Fe _{2.75} O ₄	as-prepared	2.9 ± 0.2	7123.24
	at 1.8 V _{RHE} (OER)	2.9 ± 0.2	7123.29
	after OER	2.9 ± 0.2	7123.09

EXAFS fitting parameters:

The alignment and analysis were done using Athena and the FEFFIT code.^[6-8] Fitting of EXAFS was carried out in *R*-space from 1-4.0 Å with a *k*-range of 3-9 Å⁻¹. $\chi(k)k^1$, $\chi(k)k^2$ and $\chi(k)k^3$ were fitted simultaneously. Coordination numbers *N*, interatomic distances *R*, disorder factors σ^2 , energy shifts ΔE_0 and fit quality parameters (***R factor*** in %) extracted from the EXAFS fitting of the first three peaks attributed to M-O, di- μ -oxo bridged M-M₁ and mono- μ -oxo bridged M-M₂ paths at the Co and Fe K-edge. Uncertainties of the last digit are provided in parentheses. The S_0^2 was 0.75 for all samples at Co edge and 1.0 at Fe edge as calculated by Co₃O₄ and Fe₃O₄ references. For the first path, the amplitude *A* was calculated as (6-2x), for the second path as (6-6x) and for the third path by (6+10x). x represents the fraction of metal ions occupying the tetrahedral sites of the spinel structure.

Table S6: Co₃O₄ and Fe₃O₄ reference compounds.

Reference/ R-factor	Co/Fe- Path	N	S_0^2	variable x	σ^2 (Å ²)	ΔE_0 (eV)	r (Å)	R (%)
Co ₃ O ₄	O ₁	5.33(3)	0.75(3)	0.333	0.0030(6)	0.8(5)	1.907(4)	1.7
	Co ₁	4.00(3)			0.0030(4)		2.850(4)	
	Co ₂	9.3(3)			0.0066(6)		3.361(5)	
Fe ₃ O ₄	O ₁	5.3(1)	1.0(1)	0.333	0.017(2)	-2.3(9)	1.98(1)	1.8
	Fe ₁	4.0(1)			0.010(2)		2.98(1)	
	Fe ₂	9.3(1)			0.012(1)		3.49(1)	

CoO _x	Co-Path	N	S ₀ ²	x _{Co}	σ ² (Å ²)	ΔE ₀ (eV)	r (Å)	R (%)
as-prepared	O ₁	3.7(2)	0.75(3)	0.55(9)	0.0083(9)	0.4(7)	1.943(7)	1.7
	M ₁	2.0(5)			0.004(2)		2.916(7)	
	M ₂	8.6(9)			0.048(9)		3.42(5)	
OER	O ₁	4.5(2)	0.75(3)	0.0(1)	0.006(1)	2.1(7)	1.910(7)	2.8
	M ₁	4.5(6)			0.006(2)		2.861(7)	
	M ₂	-			-		-	
after OER	O ₁	4.4(2)	0.75(3)	0.09(9)	0.0063(7)	0.1(5)	1.912(5)	0.8
	M ₁	4.1(5)			0.008(1)		2.854(6)	
	M ₂	5.1(9)			0.013(2)		3.36(9)	

Co_{2.25}Fe_{0.75}O₄	Co-Path	N	S₀²	x_{Co}	σ² (Å²)	ΔE₀ (eV)	r (Å)	R (%)
as-prepared	O ₁	3.83(8)	0.75(3)	0.44(4)	0.006(1)	-1(1)	1.93(1)	3.4
	M ₁	2.5(2)			0.006(2)		2.89(1)	
	M ₂	7.8(4)			0.019(3)		3.41(3)	
OER	O ₁	4.1(1)	0.75(3)	0.27(5)	0.0022(5)	1.0(6)	1.898(5)	1.6
	M ₁	3.3(3)			0.0032(8)		2.854(6)	
	M ₂	6.5(5)			0.016(2)		3.41(1)	
after OER	O ₁	3.98(8)	0.75(3)	0.34(4)	0.0055(5)	-0.8(5)	1.922(5)	1.1
	M ₁	3.0(2)			0.0070(9)		2.868(6)	
	M ₂	7.1(4)			0.015(1)		3.39(1)	

CoFe ₂ O ₄	Co-Path	N	S ₀ ²	x _{Co}	σ ² (Å ²)	ΔE ₀ (eV)	r (Å)	R (%)
as-prepared	O ₁	4.5(2)	0.75(3)	0.0(1)	0.005(1)	1.9(8)	2.070(8)	1.7
	M ₁	4.4(6)			0.013(2)		2.99(1)	
	M ₂	5(1)			0.015(3)		3.52(2)	
OER	O ₁	4.5(2)	0.75(3)	0.0(1)	0.011(1)	0.1(6)	1.956(9)	1.1
	M ₁	4.5(6)			0.012(1)		2.90(1)	
	M ₂	5(1)			0.014(2)		3.50(1)	
after OER	O ₁	3.6(4)	0.75(3)	0.6(2)	0.004(29)	2(1)	2.06(2)	4.0
	M ₁	2(1)			0.004(4)		2.95(2)	
	M ₂	9(2)			0.020(4)		3.56(3)	

$\text{Co}_{0.25}\text{Fe}_{2.75}\text{O}_4$	Co-Path	N	S_0^2	σ^2 (\AA^2)	ΔE_0 (eV)	r (\AA)	R (%)
as-prepared	O ₁	4.5(4)	0.75(3)	0.007(1)	0.2(7)	2.056(9)	0.7
	M ₁	4(4)		0.01(1)		2.98(4)	
	M ₂	1(2)		0.00(2)		3.49(6)	
OER	O ₁	3.0(4)	0.75(3)	0.006(2)	5.8(7)	2.02(1)	1.9
	M ₁	4.5(6)		0.01(1)		3.0(4)	
	M ₂	1(4)		0.00(3)		3.50(7)	
after OER	O ₁	4.6(6)	0.75(3)	0.017(3)	2.6(9)	1.99(1)	1.4
	M ₁	6(4)		0.018(8)		2.96(2)	
	M ₂	2(2)		0.00(1)		3.51(3)	

$\text{Co}_{2.25}\text{Fe}_{0.75}\text{O}_4$	Fe-Path	N	S_0^2	x_{Fe}	σ^2 (\AA^2)	ΔE_0 (eV)	r (\AA)	R (%)
as-prepared	O ₁	6.00(8)	1.0(1)	0.00(4)	0.0120(9)	5.2(6)	1.955(7)	1.8
	M ₁	6.0(2)			0.015(2)		2.967(8)	
	M ₂	6.0(4)			0.018(4)		3.41(1)	
OER	O ₁	5.0(1)	1.0(1)	0.52(5)	0.010(1)	5(1)	1.94(1)	2.5
	M ₁	2.9(3)			0.007(3)		2.91(1)	
	M ₂	11.2(5)			0.025(3)		3.42(3)	
after OER	O ₁	5.39(8)	1.0(1)	0.31(4)	0.010(1)	5.0(8)	1.949(9)	1.7
	M ₁	4.2(2)			0.011(2)		2.93(19)	
	M ₂	9.1(4)			0.021(3)		3.42(2)	

CoFe ₂ O ₄	Fe-Path	N	S ₀ ²	x _{Fe}	σ ² (Å ²)	ΔE ₀ (eV)	r (Å)	R (%)
as-prepared	O ₁	5.0(2)	1.0(1)	0.5(1)	0.0105(9)	3.9(7)	1.938(8)	2.2
	M ₁	3.1(6)			0.008(2)		2.96(1)	
	M ₂	11(1)			0.014(1)		3.48(1)	
OER	O ₁	5.0(2)	1.0(1)	0.5(1)	0.010(1)	5.1(8)	1.95(1)	3.0
	M ₁	3.0(6)			0.009(2)		2.963(9)	
	M ₂	11(1)			0.018(2)		3.49(1)	
after OER	O ₁	5.6(4)	1.0(1)	0.2(2)	0.0119(8)	5.0(6)	1.954(7)	1.7
	M ₁	5(1)			0.014(2)		2.982(9)	
	M ₂	8(2)			0.015(2)		3.48(1)	

$\text{Co}_{0.25}\text{Fe}_{2.75}\text{O}_4$	Fe-Path	N	S_0^2	x	$\sigma^2 (\text{\AA}^2)$	ΔE_0 (eV)	r (Å)	R (%)
as-prepared	O ₁	6.0(2)	1.0(1)	0.0(1)	0.017(1)	4.5(8)	1.95(1)	2.3
	M ₁	6.0(6)			0.017(2)		2.98(1)	
	M ₂	6(1)			0.017(3)		3.46(1)	
OER	O ₁	6.0(2)	1.0(1)	0.0(1)	0.017(1)	4.4(8)	1.94(1)	1.8
	M ₁	6.0(6)			0.017(2)		2.97(1)	
	M ₂	6(1)			0.012(3)		3.46(1)	
after OER	O ₁	6.0(2)	1.0(1)	0.0(1)	0.016(1)	3.5(7)	1.93(1)	1.7
	M ₁	6.0(6)			0.016(2)		2.97(1)	
	M ₂	6(1)			0.012(2)		3.46(1)	

III. Experimental

Table S7. Amounts of used $\text{Co}(\text{acac})_2$ and $\text{Fe}(\text{acac})_3$ for the synthesis of $\text{Co}_x\text{Fe}_{3-x}\text{O}_4$ nanoparticles.

x	Co(acac) ₂		Fe(acac) ₃	
	n / mmol	m / mg	n / mmol	m / mg
0.00	0.00	0	1.50	530
0.25	0.13	32	1.38	485
0.50	0.25	64	1.25	441
0.75	0.38	96	1.13	397
1.00	0.50	129	1.00	353
1.25	0.63	161	0.88	309
1.50	0.75	193	0.75	265
1.75	0.88	225	0.63	221
2.00	1.00	257	0.50	177
2.25	1.13	289	0.38	132
2.50	1.25	321	0.25	88
2.75	1.38	353	0.13	44
3.00	1.50	386	0.00	0

IV. References

- [1] V. Blaskov, V. Petkov, V. Rusanov, L. M. Martinez, B. Martinez, J. S. Muñoz, M. Mikhov, *J. Magn. Magn. Mater.* **1996**, *162*, 331-337.
- [2] G. A. Sawatzky, F. Van der Woude, A. H. Morrish, *Phys. Rev.* **1969**, *187*, 747-757.
- [3] G. A. Sawatzky, F. Van der Woude, A. H. Morrish, *J. Appl. Phys.* **1968**, *39*, 1204-1206.
- [4] G. Concas, G. Spano, C. Cannas, A. Musinu, D. Peddis, G. Piccaluga, *J. Magn. Magn. Mater.* **2009**, *321*, 1893-1897.
- [5] Y. Ichiyanagi, Y. Kimishima, S. Yamada, *J. Magn. Magn. Mater.* **2004**, *272-276*, E1245-E1246.
- [6] B. Ravel, M. Newville, *J. Synchrotron Radiat.* **2005**, *12*, 537-541.
- [7] M. Newville, *J. Synchrotron Radiat.* **2001**, *8*, 322-324
- [8] J. Timoshenko, A. Anspoks, A. Kalinko, A. Kuzmin, *Phys. Status Solidi A* **2015**, *212*, 265-273.